Carrier Generation and Collection in CdS/CdSe-Sensitized SnO2 Solar Cells Exhibiting Unprecedented Photocurrent Densities

ARTICLE *in* ACS NANO · MARCH 2011

Impact Factor: 12.88 · DOI: 10.1021/nn200315b · Source: PubMed

THE JOURNAL OF PHYSICAL CHEMISTRY C

Article

pubs.acs.org/JPCC

Charge Transfer Mediation Through Cu_xS. The Hole Story of CdSe in Polysulfide

James G. Radich,[†] Nevin R. Peeples,[†] Pralay K. Santra,[‡] and Prashant V. Kamat*[,†,‡]

[†]Notre Dame Radiation Laboratory, Department of Chemical & Biomolecular Engineering and [‡]Department of Chemistry & Biochemistry, University of Notre Dame, Notre Dame, Indiana 46556, United States

Supporting Information

ABSTRACT: Hole transfer to dissolved sulfide species in liquid junction CdSe quantum dot sensitized solar cells is relatively slow when compared to electron transfer from CdSe to TiO_2. Controlled exposure of cadmium chalcogenide surfaces to copper ions followed by immersion in sulfide solution promotes development of the interfacial Cu_xS layer, which mediates hole transfer to polysulfide electrolyte by collection of photogenerated holes from CdSe. In addition, Cu_xS was also found to interact directly with defect states on the CdSe surface and quench emission characteristic of electron traps resulting from selenide vacancies. Together these effects were found to work in tandem to deliver 6.6% power conversion efficiency using Mn-doped CdS and CdSe cosensitized quantum dot solar cells. Development of an n−p interfacial junction at the photoanode−electrolyte interface in quantum dot solar cells unveils new means for designing high efficiency liquid junction solar cells.

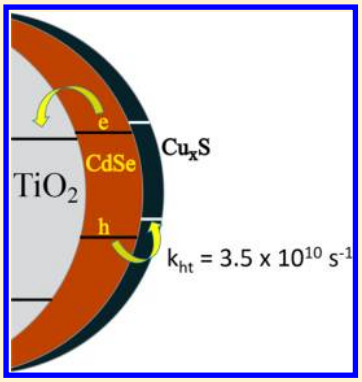

INTRODUCTION

Significant efforts to harness solar energy using nanostructured architectures have been underway for some time.[1,2] Quantum dot sensitized solar cells (QDSCs) consisting of chalcogenide sensitizers in the Grätzel construct[3] have seen significant improvements in recent years resulting from introduction of stable counter electrode materials,[4] high-loading deposition methods,[5,6] heterostructured interfaces,[7−9] and use of ternary compounds for extended light absorption.[10−12] Unlike most traditional solar cells, QDSCs operate based on principles of photoinduced electron transfer since the length scale of the photoactive materials is too small to support field-driven charge separation.[13] Use of a mesoporous metal oxide substrate such as TiO_2 as electron acceptor from absorbers such as CdS and CdSe facilitates charge transport to the transparent contact. The hole remains at the surface of the n-type absorber where the reduced species of the electrolyte donates an electron to regenerate the sensitizer. Finally, transported electrons and oxidized electrolyte species rejoin and complete the circuit at the counter electrode.

Photoinduced electron transfer from sensitizers such as CdSe to the TiO_2 matrix has been shown to occur with rate constants on the order of k_{et} = 10^{10}−10^{11} s^{-1} using pump−probe femtosecond transient absorption spectroscopy.[14−17] Meanwhile, hole transfer from visible-absorbing sensitizers to polysulfide or CuSCN is more sluggish with k_{ht} = 10^{7}−10^{9} s^{-1}.[18,19] This bottleneck in hole transfer impedes the ability to realize higher efficiency solar cells by increasing the probability of electron−hole recombination and loss of carriers before collection into the TiO_2 transport matrix. While most work has been done in tailoring the surface chemistry of CdSe quantum dots to improve excited state lifetimes and charge injection rates to TiO_2, a recent study on CdSe nanowires using a carbazole surface modifier demonstrated improved electron−hole separation via hole transfer from CdSe to carbazole.[20] Hole transfer from CdS to dibromofluorescein was also demonstrated to occur on an ultrafast time scale of 800 fs through formation of a ground state charge transfer complex.[21]

Previous reports suggest that diffusion of copper ions from use of a brass counter electrode in photoelectrochemical cells with polysulfide electrolyte deposits on CdSe single-crystal surfaces.[22,23] The notable feature of the postilluminated CdSe electrode was the placement of the Cu_xS crystals at surface defects. Following dissolution of copper ions from the brass counter electrode and subsequent deposition of the copper sulfide species on the CdSe surface, improvement in the cell was observed in the form of increased photocurrent density. This cell improvement was attributed to passivation of electron trapping sites by the copper sulfide clusters. Evidence for hole transfer from CdSe to Cu_xS in this study was elusive, leaving open the possibility of an additional component to the mechanistic role of the Cu_xS. However, in our previous work we reported bifunctional behavior in the electrocatalytic effect of Cu_2S toward both polysulfide reduction *and* oxidation,[4] suggesting the use of copper sulfide as a potential hole mediator between CdSe and polysulfide in QDSCs.

Studies incorporating p-type nanocrystalline hole-mediating components at the electrode−electrolyte interface in QDSC are

Special Issue: Michael Grätzel Festschrift

Received: November 18, 2013
Revised: February 5, 2014

   dx.doi.org/10.1021/jp4113365 | *J. Phys. Chem. C* XXXX, XXX, XXX−XXX

rare, or possibly nonexistent. Here we utilize a simple successive ionic layer adsorption and reaction (SILAR) approach to develop the Cu_xS layer at the CdSe−polysulfide interface. Integration of this interfacial layer into CdSe-based QDSCs facilitated improvements in the photoelectrochemical performance. We probed the excited state interactions between CdSe and Cu_xS in aqueous medium with reverse micelles using emission quenching and on mesoscopic TiO_2 films using transient absorption spectroscopy. The results reveal that the Cu_xS layer participates as a hole mediator from CdSe to polysulfide and demonstrates direct interaction of Cu_xS with defect states in CdSe. The results highlight a new approach toward improving the efficiency of QDSCs by incorporating an interfacial hole transfer layer to segregate n-type absorber (viz., CdSe) and electrolyte species (viz., polysulfide) and thereby improve charge separation.

EXPERIMENTAL SECTION

Materials and Methods. QDSCs were constructed using a fluorine-doped tin oxide (FTO) substrate. FTO was cut to the appropriate size and subjected to ultrasonication in detergent solution for 30 min, followed by deionized water (DI) and ethanol rinse with air drying. Photoanode substrates were immersed in $TiCl_4$ solution (40 mM) and heated to 70 °C for 30 min to deposit a blocking layer, followed by another DI and ethanol rinse and air drying. Solaronix Ti-Nanoxide T/SP TiO_2 paste was bladed onto a 0.25 cm^2 active area and dried at ambient temperature for 1 h and 80 °C for 1 h, then annealed at 500 °C for 1 h. JBC Catalysts and Chemicals Ltd. PST-400C TiO_2 scattering layer was then deposited with identical steps. Finally, a post-$TiCl_4$ solution (40 mM) treatment was rendered followed by 30 min final heat treatment at 500 °C.

Co-sensitized TiO_2 photoanodes were prepared via SILAR by first using manganese acetate-doped (0.075 M) cadmium sulfate (0.1 M) solution and sodium sulfide (0.1 M) solution (1:1 DI/methanol) for five cycles of the Mn-doped CdS layer (1 min immersion).[24] CdSe SILAR precursor solutions consisted of 0.03 M $CdNO_3$ in ethanol and sodium borohydride-reduced SeO_2 solution for 0.03 M Se^{2-} solution in ethanol. In all, eight cycles of CdSe were deposited (30 s immersion) under nitrogen environment. Cu_xS was incorporated by preparing Cu^+ aqueous solution by first mixing 40 mg of anhydrous $CuSO_4$ in 2 mL of DI and 250 mg of $Na_2S_2O_3$ in 10 mL of DI. Once dissolved the Cu solution was mixed with thiosulfate solution which resulted in transient greenish color followed by a clear solution. Electrodes were immersed from 2 to 10 s followed by 1 min immersion in 0.1 M Na_2S aqueous solution. $Zn(NO_3)_2$ and Na_2S solutions (0.1 M) were used to incorporate the ZnS blocking layer via two SILAR cycles (1 min immersion).

Polysulfide electrolyte was prepared by dissolving 2 M Na_2S and 2 M S in DI. Counter electrodes were constructed by blading reduced graphene oxide−Cu_2S paste onto cleaned FTO, drying under vacuum for at least 4 h at 110 °C, and immersing in polysulfide solution for 1 h.[4] QDSCs were realized by placing a Parafilm spacer over the counter electrode, dropping 1−2 drops of electrolyte on each electrode, sandwiching electrodes together, and securing with binder clips.

CdSe quantum dots and Cu_xS nanocrystals were synthesized in aqueous reverse micelles by first preparing 0.394 M sodium dioctyl sulfosuccinate (AOT)/heptane solution. Aqueous $CdSO_4$ (0.1 M) and Na_2SeSO_3 (0.1 M) served as Cd and Se precursor sources for CdSe quantum dots. Na_2SeSO_3 was prepared by refluxing Se powder (0.395 g) in 50 mL of Na_2SO_3 (2.4 g) solution for 3 h. Cu_xS precursors consisted of a Cu−thiosulfate complex as described above and Na_2S. CdSe precursor solutions (1 mL of $CdSO_4$, 0.9 mL of Na_2SeSO_3 + 0.1 mL of DI) were mixed separately with 9 mL of AOT/heptane solution and sonicated for 10 min until clear. Identical treatment for Cu_xS precursors followed. Equal volumes of these solutions were mixed in separate vials and were allowed to sit for at least 24 h prior to use in further experiments. The Cu_xS crystals were washed three times by precipitating with DI and resuspending in AOT/heptane to remove residual precursor solutions that can interfere with photoinduced charge transfer measurements. The final concentration of Cu_xS in AOT/heptane solution was 240 μg/mL.

Surface electron traps were induced into CdSe quantum dots in reverse micelles by sonicating the vial containing the two individual precursors for 20 min, after which the temperature of the solution rose to 35 °C. CdSe with band edge emission was synthesized by cooling the precursors before mixing to 4 °C and holding at this temperature after mixing for 24 h. All precursor solutions and postmixed solutions were degassed with N_2 sufficiently to remove residual O_2 from the vials.

Materials Characterization. Scanning electron micrographs were obtained using Magellan 400 FESEM with a Bruker X-ray detector. Energy-dispersive X-ray spectroscopy (EDXS) was performed by inserting an X-ray detector and holding the electron beam over the selected sample area for 1 min. X-ray mapping was followed by selecting the Cu Kα peak and S Lα peak and collecting an average of two scans. Scanning electron micrographs were obtained on CdSe- or CdSe/Cu_xS-sensitized TiO_2 electrodes (without CdS or ZnS).

Photoelectrochemical Measurements. Photoelectrochemical measurements were carried out using a Princeton Applied Research 2273 (PARstat) potentiostat in a two-electrode configuration. The active area of the photoanode ranged from 0.18 to 0.22 cm^2. A 300 W Xe lamp with an AM 1.5G filter was used to irradiate cells at 100 mW/cm^2. Current−voltage (J−V) measurements were recorded by sweeping potential from 0.05 to −0.55 V at 10 mV/s. Voltage decay measurements were carried out by irradiating the cell for 30 s followed by switching off excitation and monitoring the decay in voltage. Internal photon-to-carrier conversion efficiency (IPCE) was measured with a Newport Oriel QE/IPCE measurement kit with a silicon detector.

Optical Measurements. A Cary 50 Bio spectrophotometer was used to record UV−visible absorption spectra of CdSe- or CdSe/Cu_xS-sensitized TiO_2 electrode (without CdS or ZnS). Steady state photoluminescence measurements were recorded using a Jobin Yvon Fluorolog. Transient absorption (TA) measurements were recorded using a Clark MXR CPA-2010 (775 nm fundamental, 1 mJ/pulse, 130 fs fwhm, 1 kHz repetition rate) incorporating Helios software provided by Ultrafast Systems. The pump beam (95% of the fundamental frequency doubled to 387 nm) and the probe beam (the remaining 5% focused onto a Sapphire crystal to generate a white light continuum) are incident on CdSe films grown via eight cycles of SILAR (with Cu_xS treatment on one) on ∼500 nm mesoscopic TiO_2 deposited on FTO by spinning 2.5:1 ethanol:Dyesol 18NR-T and sintering.

RESULTS AND DISCUSSION

Photoanode Surface Characterization. Deposition of interfacial Cu_xS at the CdSe-based photoanode was accom-

dx.doi.org/10.1021/jp4113365 | J. Phys. Chem. C XXXX, XXX, XXX−XXX

Scheme 1. Synthesis of QDSC Photoanode Containing a n−p Nanoheterojunction between CdSe and Cu_xS[a]

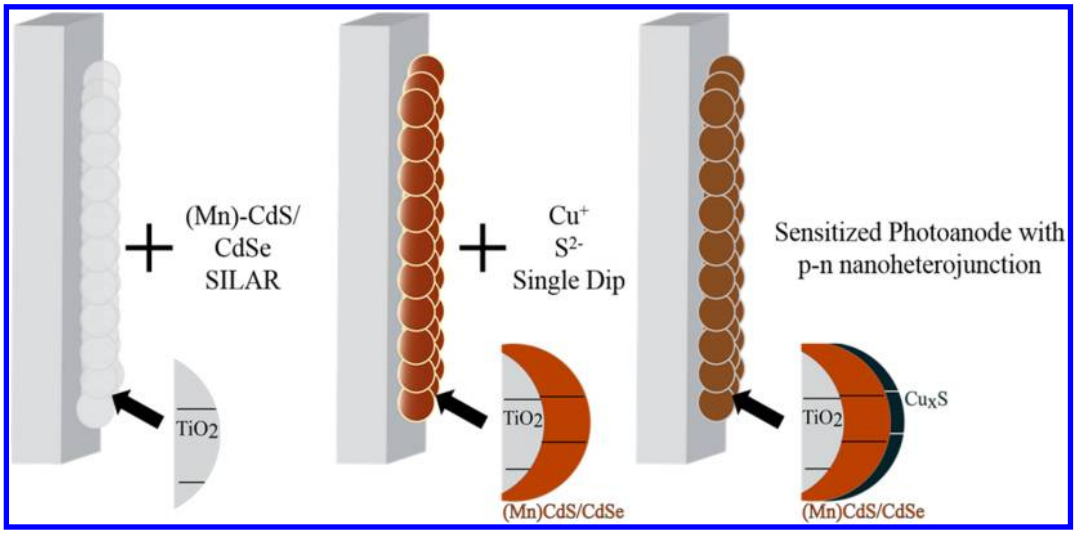

[a]TiO_2 electrodes were first sensitized with five cycles of Mn-doped CdS, followed by eight cycles of CdSe. Immersion of the CdSe interface in Cu^+ and S^{2-} solution facilitated development of the Cu_xS layer accompanied by ∼100 nm diameter hexagonal platelets dispersed over the electrode surface.

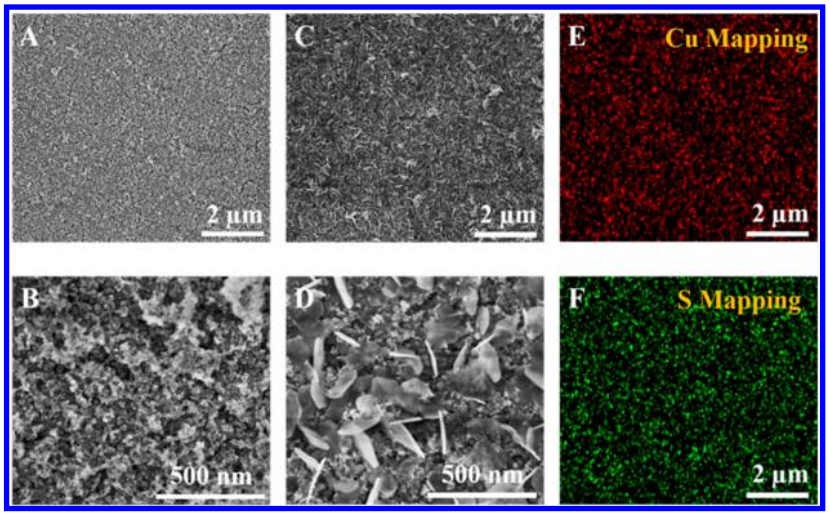

Figure 1. Scanning electron micrographs of CdSe-sensitized (A, B) and CdSe−Cu_xS-sensitized (C, D) TiO_2 electrodes illustrating the deposition of Cu_xS platelets onto the CdSe surface. Cu_xS was deposited through the sequential dipping method. (E) and (F) Illustrate the Cu and S coverage of the photoanode in (C) via EDXS X-ray mapping.

plished by exploiting a displacement reaction between CdSe and copper ions[25] through dipping the CdSe-sensitized photoanode into thiosulfate-stabilized Cu^+ solution, followed by dipping in sulfide solution. The reaction between the CdSe surface and copper ions facilitated the development of the interfacial Cu_xS layer. Scheme 1 depicts the synthetic approach to forming the CdSe−Cu_xS heterostructure. Realistically, the interfacial layer likely consists of some degree of ternary $Cu_xSe_yS_{(1-y)}$ depending on the level of Cd displacement during immersion. For simplicity we refer to this interfacial layer as Cu_xS since interaction between Cu and Se is most likely limited to Se^{2-} ions on the CdSe surface.

We investigated the CdSe−Cu_xS interfacial characteristics using scanning electron microscopy. Typical mesoporous sensitized TiO_2 electrode characteristics are evident in Figures 1A and 1B and demonstrate the excellent surface coverage of the TiO_2 network with CdSe. Figures 1C and 1D display hexagonal-like 2-D structures of Cu_xS at ca. 100 nm in diameter protruding from the CdSe−TiO_2 network. These hexagonal features are consistent with previous Cu_2S[4] and Cu_xS[23] morphologies, which offer further evidence of minimal incorporation of Se into final Cu_xS nanostructures since Cu_xS via displacement of Cd^{2+} should develop an interfacial layer rather than precipitates. Energy-dispersive X-ray spectra conclusively demonstrate the presence of Cu_xS species in the electrode containing these platelets (Figure S1, Supporting Information). Analysis of Cu/S and Cd/Se atomic ratios suggests a small level of Cu−Cd exchange upon immersion of the CdSe electrode into Cu^+ solution supporting the assertion of deposition of a mixed interfacial layer via Cd^{2+} displacement *and* Cu_xS precipitates (Figure S1, Supporting Information). X-ray maps of Cu (Figure 1E) and S (Figure 1F) of the image in Figure 1C illustrate the homogeneous distribution of Cu_xS decorating the surface of the electrode.

Photoelectrochemical Performance. To probe the influence of Cu^+ exchange on the electrode absorption

dx.doi.org/10.1021/jp4113365 | J. Phys. Chem. C XXXX, XXX, XXX−XXX

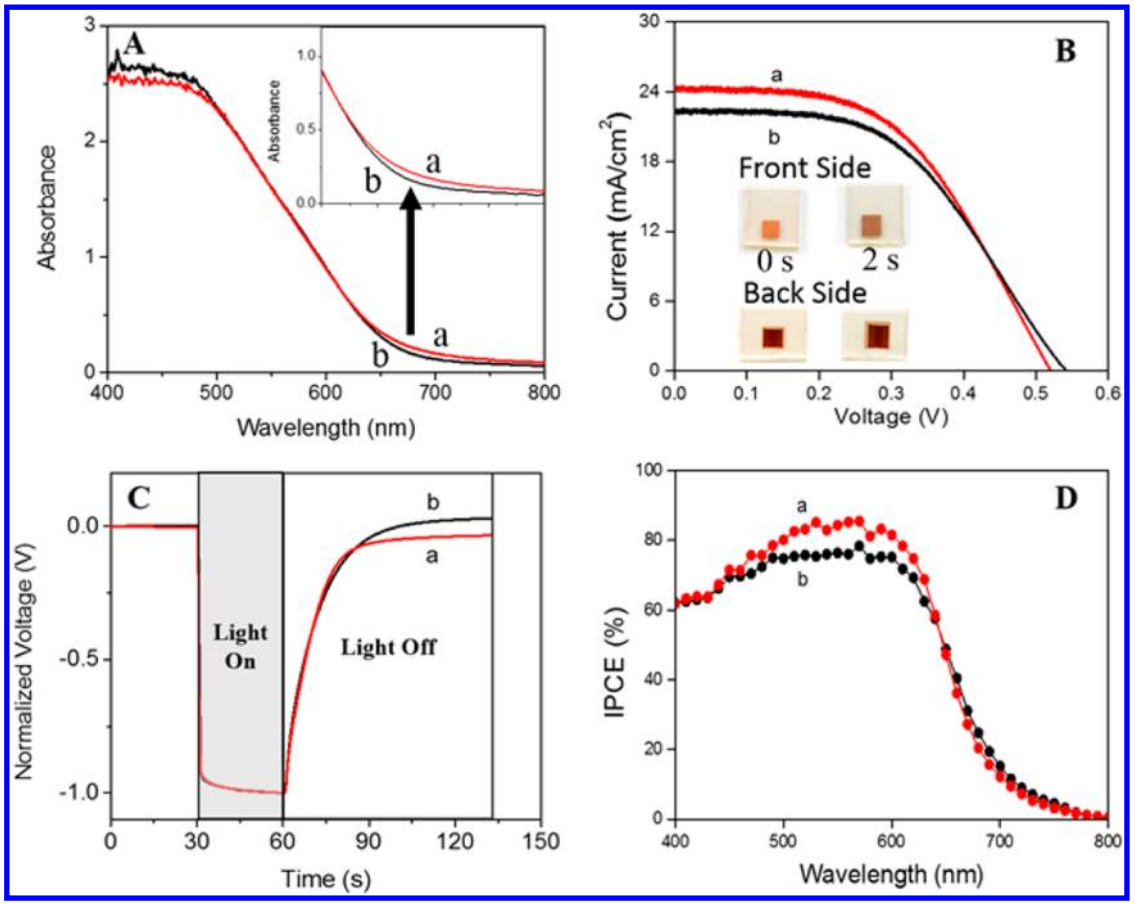

Figure 2. (A) Absorption characteristics of the CdSe-sensitized (8 cycle) TiO_2 electrode (a) with and (b) without Cu_xS treatment. (B–D) Photoelectrochemical characteristics of the (Mn)CdS/CdSe–Cu_xS electrode in a QDSC (RGO/Cu_2S counter electrode, aqueous 2 M S^{2-}/2 M S as redox electrolyte). The performances of the optimized (Mn)CdS/CdSe–Cu_xS electrode (a) are compared with (Mn)CdS/CdSe (b) in QDSC under 1.5 AM simulated solar irradiation.

properties, we prepared a TiO_2 film coated with CdSe on an OTE. The OTE/TiO_2/CdSe electrode was briefly exposed to Cu^+ and S^{2-} solutions (2 s). The resulting changes in electrode absorption are shown in Figure 2A. The slight increase in absorbance at wavelengths greater than 700 nm is attributed to the deposition of Cu_xS on the CdSe surface. This extended absorption is also apparent visually as depicted in Figure 2B (photograph insets). No significant changes in CdSe absorption characteristics, specifically at absorption onset wavelengths, were observed, owing to minimal Cd–Cu exchange upon immersion in Cu^+ solution. We expect the absorption spectrum of CdSe to be especially sensitive to surface exchange of Cd via Cu considering the extremely small dimensions of quantized CdSe domains.

Next we incorporated (Mn)CdS/CdSe–Cu_xS (Mn-doped CdS) and (Mn)CdS/CdSe into mesoscopic TiO_2 architectures and employed them as photoanodes in QDSCs to evaluate the contributions of the Cu_xS toward photoelectrochemical performance in QDSCs. These solar cells will be referred to as Cu_xS-based QDSC and control, respectively. The photoelectrochemical characteristics were evaluated by subjecting the QDSC to AM 1.5G irradiation. Measurements of J–V characteristics, voltage decay, and external quantum efficiency were recorded on Cu_xS-based QDSCs and were compared to a control without Cu_xS treatment. The results are shown in Figures 2B–2D, respectively. Photoelectrochemical characteristics of QDSCs with extended deposition times for Cu_xS as well as photocurrent stability measurement of the optimized QDSC are provided in Figure S2 (Supporting Information).

An 11% increase (9.3 ± 1.2% over three sets) in photocurrent was measured in the champion Cu_xS-based QDSC (24.5 mA/cm^2) relative to the control (22 mA/cm^2). The increase in photocurrent was accompanied by a slight drop in V_{oc} from 0.54 V (control) to 0.52 V (Cu_xS) and a similar fill factor of 0.5 (control) and 0.52 (Cu_xS). These parameters yield power conversion efficiency values of 6.6% for the Cu_xS-based QDSC (5.7% masked) and 5.9% for control (5.2% masked). Voltage decay following elimination of the excitation source can be considered a measure of electron recombination with oxidized electrolyte species.[26] The voltage–time plot in Figure 2C shows nearly identical decay of carriers upon removal of light excitation source. Incident photon-to-carrier conversion efficiency (IPCE) measurements presented in Figure 2D resolve the source of additional photocurrent to arise from higher photon conversion in the visible range from ca. 475 to 650 nm.

Since the deposition of Cu_xS extended the absorption range of the CdSe electrode (Figure 2A), we note the lack of photocurrent action at these wavelengths beyond the CdSe onset (viz., 700–800 nm). If a photoactive role by the Cu_xS is responsible for the measured improvement in photoelectrochemical performance, IPCE results imply that Cu_xS contributes only in midvisible regions with favorable photon energy for electron injection into CdSe. Electrons converted

dx.doi.org/10.1021/jp4113365 | J. Phys. Chem. C XXXX, XXX, XXX–XXX

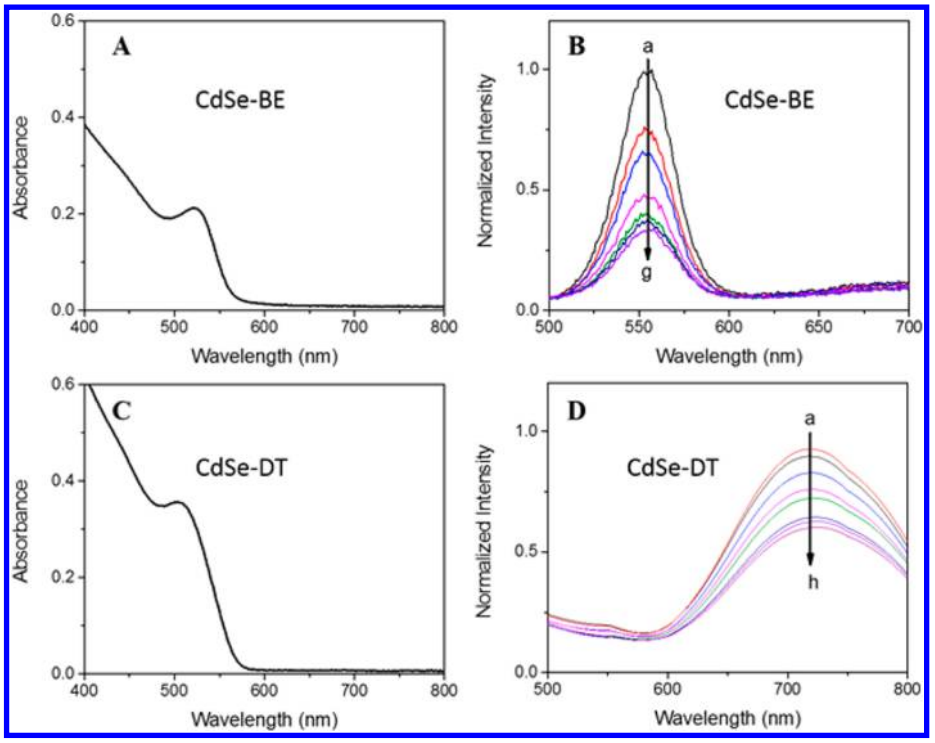

Figure 3. Steady state absorption (A and C) and emission spectra (B and D) of colloidal CdSe in reverse micelles. Labels CdSe−BE and CdSe−DT represent quantum dots with band edge and deep trap emission characteristics, respectively. Sequential additions of 48 μg of Cu_xS using 200 μL of 240 μg/mL Cu_xS solution to CdSe solution is represented by traces (a)−(h) where trace (a) is 0 μg of Cu_xS. Band edge emission is shown in (B) and deep trap emission in (D). Excitation wavelength for emission experiments was 387 nm.

from lower-energy photons near the band edge of Cu_2S in CdS−Cu_2S solid state solar cells are known to resist injection into CdS as a result of the energy barrier developed at the CdS−Cu_2S interface.[27]

One can also envision two distinct nonphotoactive roles of Cu_xS in QDSC: (1) Catalytic shuttling of holes from CdSe to polysulfide which would provide enhanced charge separation and facilitate improved photocurrent density under irradiation and (2) remediation of surface defects that induce charge trapping. If the latter argument is true one would expect increased excited state lifetime through removal of electron traps that facilitate recombination.[15,22] Thus, it is unclear at this stage if the increased photocurrent obtained in the visible region in IPCE measurements shown in Figure 2D arises from improved charge separation via surface passivation, hole transfer from CdSe to Cu_xS, photoinduced electron transfer from Cu_xS to CdSe originating from midvisible photons, or some combination of these effects. To clarify the role of Cu_xS in QDSC we probed the interfacial charge transfer processes in CdSe and Cu_xS systems.

CdSe−Cu_xS Excited State Interactions in Confined Media. Use of reverse micelles to study excited state interactions between semiconductors, quantum dots, and metal nanoparticles has been effective in enabling the mapping of charge transfer events.[28−30] Reverse micelles consist of a size-tunable polar core surrounded by nonpolar solvent and facilitate size-controlled particle synthesis. In this study the water−heptane system coordinated with sodium dioctyl sulfosuccinate (AOT) was used as a result of its ability to form spherical water pools.[31] The molar ratio of water to AOT dictates the size of the water pool, which was ca. 5 nm in this study. Thus, by synthesizing the CdSe and Cu_xS in reverse micelles we were able to control the particle size and probe the excited state interactions between CdSe and Cu_xS in aqueous media, resembling that of the electrolyte solvent of the QDSC.

We first probed the excited state interactions between CdSe and Cu_xS using steady state emission spectroscopy. Emission quenching is a good probe to monitor the excited state interaction between the emissive material and an electron donor or acceptor. We utilized two synthetic approaches to prepare CdSe quantum dot samples, one predominantly with band edge emission (CdSe-BE) and the other with deep trap emission arising from selenium vacancies (CdSe-DT).[32] The CdSe colloids in reverse micelles prepared at lower temperature (4 °C) yield high-quality quantum dots dominated by band edge emission with maximum at 560 nm. If precursor solutions in reverse micelles are sonicated at 35 °C for 15 min, we obtain CdSe colloids having particle size similar to that obtained at 4 °C but with large density of surface defects. The dominance of surface defects is evident from the broad, deep trap emission (maximum at 720 nm). This approach enabled us to probe the interaction of Cu_xS with two different CdSe colloids having different density of deep trap states. Figures 3A and 3B depict the absorption spectrum of the CdSe−BE colloids and the corresponding quenching of band edge emission upon incremental addition of Cu_xS, respectively. Figures 3C and 3D show the absorption spectrum of CdSe−DT and the corresponding quenching deep trap emission upon incremental additions of Cu_xS.

Both the band gap and trap emission of the CdSe emission are quenched by Cu_xS. CdSe−BE exhibited ca. 70% quench of the band edge emission with CdSe-DT showing ca. 40% quench in trap emission after cumulative addition of 288 μg and 336 μg of Cu_xS, respectively. The quenching of the band edge and deep trap emission implies that Cu_xS interacts with

dx.doi.org/10.1021/jp4113365 | J. Phys. Chem. C XXXX, XXX, XXX−XXX

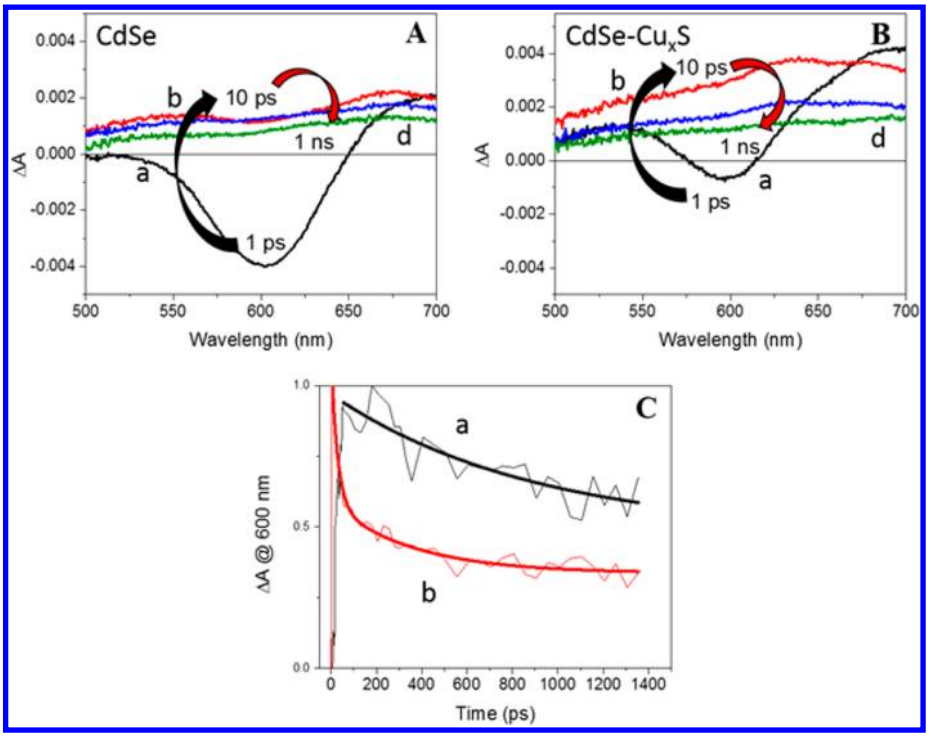

Figure 4. Transient absorption spectra for CdSe (A) and CdSe−Cu_xS (B) at different times following laser excitation using 387 nm pulse. Trace (a) 1 ps following laser pulse, (b) 10 ps, (d) 1 ns. Traces in (C) represent relaxation of the induced absorption signal in CdSe (a) and CdSe−Cu_xS (b).

the CdSe surface and influences the excited state deactivation processes from the band edge and surface states.

As a control experiment we verified quenching was a result of Cu_xS interaction with CdSe and not Cd^{2+} displacement via residual Cu^+ ions in aqueous micelles by measuring the absorbance of the CdSe−Cu_xS mixed solution after band edge quenching experiments. The high sensitivity of the CdSe quantum dot absorption feature at the characteristic first excitonic peak provides a means to assess changes in the CdSe quantum dot surface. No changes in CdSe absorption were observed at these low Cu^+ concentrations, which asserts quenching does not result from residual Cu^+ in micelle solution. (Figure S3, Supporting Information). Also, quenching with AOT/heptane−water solution was negligible, and the absorbance of the Cu_xS at the highest concentration was less than 10% at the excitation wavelength (Figure S3, Supporting Information). The interaction observed in the present experiments at the semiconductor interface between CdSe and Cu_xS shows that Cu_xS can play a dominant role in determining the excited state decay pathway of CdSe.

It should be noted that Cu_xS is known to possess p-type behavior. If indeed Cu_xS interacts with excited CdSe by capturing holes, it can serve as a hole mediator and promote charge separation. Induced absorbance arising from sulfide radical ($S^{-\bullet}$) and selenide radical ($Se^{-\bullet}$) species has been observed from hole trapping on metal chalcogenide surfaces or oxidation of organic molecules in studies involving pulse radiolysis[33,34] and pulsed laser spectroscopy.[35−38] The radical species generally exhibit characteristic broad features from 450 to 650 nm. Femtosecond and nanosecond transient absorption spectroscopy were carried out to identify the hole transfer process in CdSe and CdSe−Cu_xS deposited onto mesoscopic TiO_2 films. We used a 500 nm TiO_2 layer with CdSe and CdSe−Cu_xS SILAR to enable transmission of probe light for optical studies while mimicking the QDSC sensitizer deposition method.

When CdSe films are excited with 387 nm (or 355 nm) laser pulse, we expect the formation of the $Se^{-\bullet}$ radical as a result of hole trapping on the CdSe surface. If Cu_xS is present at the interface it can participate in the hole transfer process and lead to the additional formation of the $S^{-\bullet}$ species (eqs 1−4). We specifically focused on differences in induced absorption decay kinetics between the CdSe and CdSe−Cu_xS sensitized films in femtosecond pulsed laser experiments. Figure 4 shows the femtosecond transient absorption spectra (Figures 4A and 4B) and relaxation kinetics for CdSe and CdSe−Cu_xS (Figure 4C).

$$\mathrm{CdSe} + h\upsilon \rightarrow \mathrm{CdSe}(e - h) \quad (1)$$

$$\mathrm{CdSe}(e - h) + \mathrm{TiO_2} \rightarrow \mathrm{CdSe}(h) + \mathrm{TiO_2}(e) \quad (2)$$

$$\mathrm{CdSe}(h) \rightarrow \mathrm{CdSe}^{-\bullet} \quad (3)$$

$$\mathrm{CdSe}^{-\bullet} + \mathrm{Cu_xS} \rightarrow \mathrm{Cu_xS}^{-\bullet} \quad (4)$$

The time-resolved difference absorption spectra recorded in Figures 4A and 4B illustrate several characteristic features of the CdSe and CdSe−Cu_xS films. The CdSe film showed a bleaching at early times (see spectrum a, Figure 4A, recorded 1 ps after the pulse) which is followed by the growth of induced absorption signal. The induced absorption exhibits features characteristic of trapped holes on the surface to give $Se^{-\bullet}$.[37] This positive absorption signal decays via single exponential behavior within the time window of 1.6 ns (trace a Figure 4C). The CdSe−Cu_xS film demonstrated smaller bleaching signal after 1 ps, followed by a rapid rise in positive absorption signal. The magnitude of the induced absorption was greater in CdSe−Cu_xS films than CdSe films, implying additional hole trapping sites are formed during deposition of Cu_xS onto CdSe via a displacement reaction between Cu^+ and Cd^{2+}. The spectra

dx.doi.org/10.1021/jp4113365 | J. Phys. Chem. C XXXX, XXX, XXX−XXX

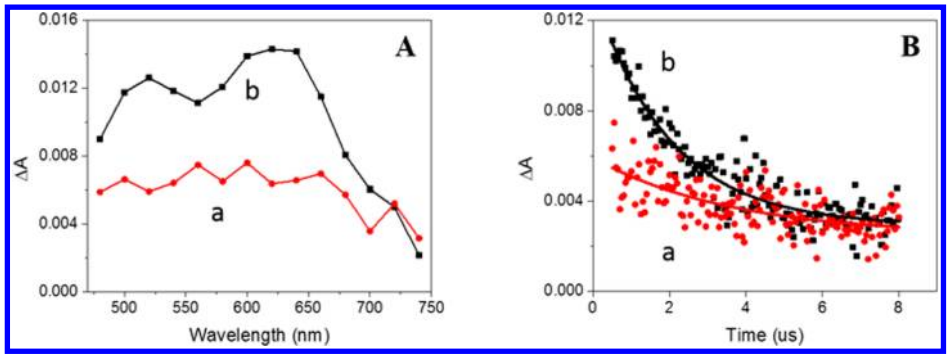

Figure 5. Nanosecond flash photolysis spectral features (A) and decay at 560 nm (B) of CdSe (a) and CdSe−Cu_xS (b) films. The spectra represent absorption values immediately following 355 nm laser pulse. Lifetimes were obtained using traces in (B) using single exponential kinetic analysis and were used to calculate k_{rec}.

Scheme 2. Transient Absorption Spectroscopy of CdSe and CdSe−Cu_xS Films Demonstrates the Hole Trapping and Transfer Processes[a]

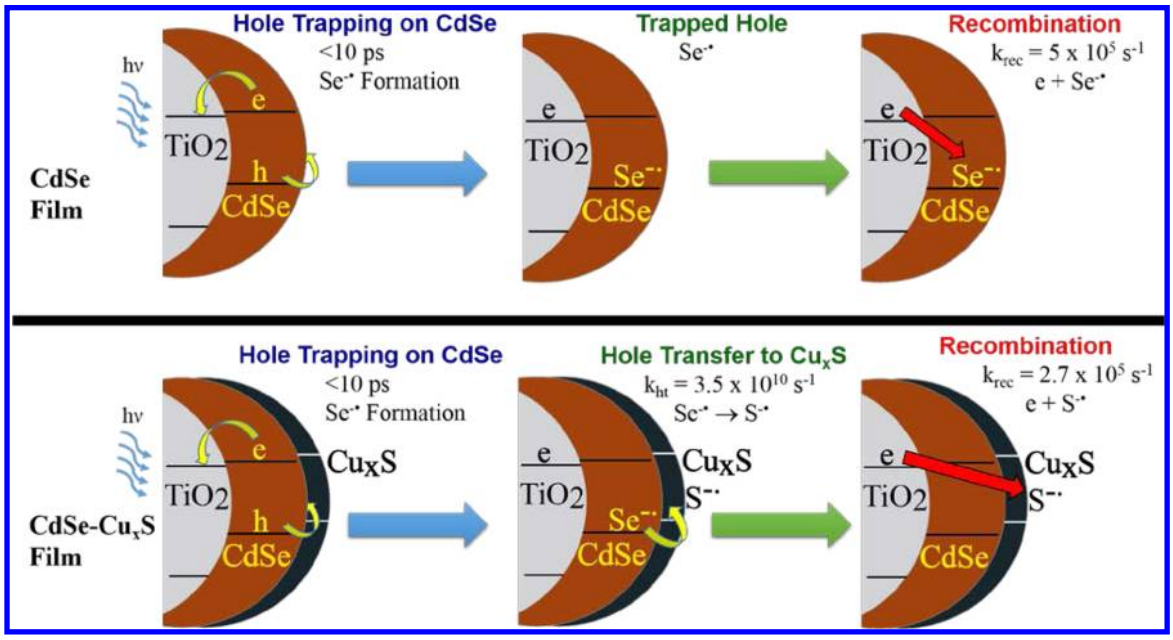

[a]The initial hole trapping occurs within the first 10 ps following laser pulse excitation. The transfer of holes from CdSe to Cu_xS was monitored by following the transient absorption of the respective radical species ($Se^{-\bullet}$ and $S^{-\bullet}$) arising from hole trapping on CdSe and Cu_xS, respectively. Hole transfer from CdSe to Cu_xS facilitated an improved charge-separated state as evidenced by the slower recombination rate for electrons and holes.

recorded in the duration of 0−1 ps for CdSe and CdSe−Cu_xS films as well as Cu_xS alone are compared in Figures S4 and S5, respectively, in the Supporting Information.

The decay of the induced absorption in the CdSe−Cu_xS film monitored at 600 nm on the picosecond time scale (trace a Figure 4C) exhibited a biexponential behavior compared with single exponential behavior in CdSe film (trace b Figure 4C). Biexponential fitting is relevant to heterogeneous systems.[15,18,39] The presence of the fast decay component indicated that an additional reaction pathway contributes to the decay of $Se^{-\bullet}$ (reaction 4). If hole transfer from CdSe to Cu_xS is the only additional pathway contributing to the decay of $Se^{-\bullet}$, the rate constant for the hole transfer (k_{ht}) process can be calculated from the difference between the inverse of the two lifetimes (τ_0 and τ) obtained with CdSe vs CdSe−Cu_xS films (eqs 5 and 6).

$$1/\tau_0(\text{CdSe}) = k_{rec} \text{ and } 1/\tau_0(\text{CdSe–Cu}_x\text{S}) = k_{rec} + k_{ht} \quad (5)$$

$$1/\tau(\text{CdSe–Cu}_x\text{S}) - 1/\tau_0(\text{CdSe}) = k_{rec} + k_{ht} - k_{rec} = k_{ht} \quad (6)$$

The rate constants for the respective processes are represented by k with k_{rec} and k_{ht} referring to the rate of electron−hole recombination and hole transfer from CdSe to Cu_xS, respectively. The lifetime of the fast component in the CdSe−Cu_xS kinetic trace (τ) was calculated to be τ = 28 ps after fitting the trace to a biexponential kinetic analysis. The lifetime (τ_0) of the decay observed in the CdSe film was obtained by fitting to a single exponential kinetic analysis and was calculated to be τ = 895 ps. The difference of the reciprocal lifetimes for the two processes (eq 6) yields a hole transfer rate constant of $k_{ht} = 3.48 \times 10^{10}$ s^{-1}. This hole transfer rate constant is significantly faster than the rate constant (5.9×10^8 s^{-1}) obtained in a Sb_2S_3−CuSCN system[18] and comparable to the CdS−squaraine dye system (1.7×10^{10} s^{-1}).[40]

To monitor the fate of the $Se^{-\bullet}$ and $S^{-\bullet}$ in CdSe and CdSe−Cu_xS films at longer times, we carried out nanosecond laser

dx.doi.org/10.1021/jp4113365 | J. Phys. Chem. C XXXX, XXX, XXX−XXX

flash photolysis measurements. Figure 5A depicts the difference absorption spectra for CdSe and CdSe−Cu_xS films recorded following 355 nm laser pulse excitation. Distinct differences in the shape of the spectra between the two films are apparent as the transient species produced in these films correspond to $Se^{-\bullet}$ and $S^{-\bullet}$, respectively. We can also monitor the survivability of the trapped hole from the lifetime of absorption decay of the transient species ($Se^{-\bullet}$ and $S^{-\bullet}$) on the microsecond time scale. At longer times these species decay as they recombine with the trapped electrons. The obvious question is whether the hole transfer to Cu_xS in CdSe−Cu_xS film suppresses the recombination process.

Transient absorption decay at 560 nm for these two transients is shown in Figure 5B. The decay of the $Se^{-\bullet}$ (τ = 1.99 μs, standard error 0.12 μs) proceeds at a higher rate in CdSe film than that of the $S^{-\bullet}$ (τ = 3.47 μs, standard error 0.97 μs) in CdSe−Cu_xS film. At the longer times depicted in Figure 5B we can attribute the single exponential decay features to recombination of electrons and holes in the film. The lifetimes obtained after fitting to single exponential kinetic analysis can then be used to calculate the electron−hole recombination rate constant, k_{rec}, by taking the reciprocal of the respective lifetimes. The lifetimes correspond to recombination rate constants of $k_{rec} = 5.0 \times 10^5\ s^{-1}$ for CdSe film and $k_{rec} = 2.7 \times 10^5\ s^{-1}$ for CdSe−Cu_xS film. This trend is similar at other wavelengths as shown in the time-resolved spectra in Figure S6 (Supporting Information).

The slower decay of the CdSe−Cu_xS transient signal in the nanosecond experiments (Figure 5B) demonstrates that the surface modification with Cu_xS suppresses the back electron transfer process, providing the evidence for superior photoelectrochemical performance seen in QDSCs.

The interfacial charge transfer processes occurring at the CdSe and CdSe−Cu_xS are illustrated in Scheme 2. The major difference in these two films is the Cu_xS, which facilitates better charge separation by scavenging the holes trapped at the CdSe surface. Quick transfer of hole and suppression of recombination with the electrons is critical in improving the performance of QDSCs.

CONCLUSIONS

By employing the spectroscopic measurements, we have succeeded in establishing the role of Cu_xS as a good hole mediator and thus offer new opportunities to improve the interfacial charge transfer kinetics in QDSCs. These spectroscopic measurements confirm previous assertion of interaction of Cu_xS with surface electron traps while further elucidating the Cu_xS role in mediating transfer of CdSe photogenerated holes to polysulfide electrolyte. The measured hole transfer rate constant from excited CdSe into Cu_xS was $k_{ht} = 3.48 \times 10^{10}\ s^{-1}$. The recombination between the electron and trapped hole in CdSe−Cu_xS film ($k_{rec} = 2.7 \times 10^5\ s^{-1}$) was slower compared to CdSe ($k_{rec} = 5 \times 10^5\ s^{-1}$). We thus attribute the improved performance of the QDSC constructed with the Cu_xS interfacial layer to the slower rate of recombination assisted by the Cu_xS interfacial layer. The results presented in this study offer new strategies toward introduction of an n−p nanoheterojunction at the photoanode−electrolyte interface.

ASSOCIATED CONTENT

Supporting Information

EDXS spectra and compositional ratios for Cu, S, Cd, and Se, photoelectrochemical performance of QDSCs constructed with varying dipping times for Cu_xS deposition as well as photocurrent stability of optimized Mn-doped CdS/CdSe/Cu_xS/ZnS solar cell, quenching experiments with AOT/heptane−water solution, absorption characteristics of Cu_xS at highest quenching concentration, absorption spectra of CdSe before and after quenching experiments, decay of the CdSe and CdSe−Cu_xS films on the microsecond time scale, transient spectra for CdSe and CdSe−Cu_xS films between 0 and 1 ps, and blank Cu_xS transient absorption data. This material is available free of charge via the Internet at http://pubs.acs.org.

AUTHOR INFORMATION

Corresponding Author

*E-mail: pkamat@nd.edu.

Notes

The authors declare no competing financial interest.

ACKNOWLEDGMENTS

The research described herein was supported by the Division of Chemical Sciences, Geosciences, and Biosciences, Office of Basic Energy Sciences of the U.S. Department of Energy through Award DE-FC02-04ER15533 and by the Jana & Patrick Eilers Energy Research Fellowship awarded to J.R. We also thank Doug Hines for assistance with transient absorption spectroscopy experiments and data interpretation. This is contribution number NDRL No. 4996 from the Notre Dame Radiation Laboratory.

REFERENCES

(1) Shalom, M.; Buhbut, S.; Tirosh, S.; Zaban, A. Design Rules for High-Efficiency Quantum-Dot-Sensitized Solar Cells: A Multilayer Approach. *J. Phys. Chem. Lett.* **2012**, *3* (17), 2436−2441.

(2) Kamat, P. V. Quantum Dot Solar Cells. The Next Big Thing in Photovoltaics. *J. Phys. Chem. Lett.* **2013**, *4* (6), 908−918.

(3) O'Regan, B.; Gratzel, M. A Low-Cost, High-Efficiency Solar-Cell Based on Dye-Sensitized Colloidal TiO_2 Films. *Nature* **1991**, *353* (6346), 737−740.

(4) Radich, J. G.; Dwyer, R.; Kamat, P. V. Cu_2S-Reduced Graphene Oxide Composite for High-Efficiency Quantum Dot Solar Cells. Overcoming the Redox Limitations of Polysulfide at the Counter Electrode. *J. Phys. Chem. Lett.* **2011**, *2* (19), 2453−2460.

(5) Lee, H.; Wang, M. K.; Chen, P.; Gamelin, D. R.; Zakeeruddin, S. M.; Gratzel, M.; Nazeeruddin, M. K. Efficient CdSe Quantum Dot-Sensitized Solar Cells Prepared by an Improved Successive Ionic Layer Adsorption and Reaction Process. *Nano Lett.* **2009**, *9* (12), 4221−4227.

(6) Lee, Y.-L.; Huang, B.-M.; Chien, H.-T. Highly Efficient CdSe-Sensitized TiO_2 Photoelectrode for Quantum-Dot-Sensitized Solar Cell Applications. *Chem. Mater.* **2008**, *20* (22), 6903−6905.

(7) Niitsoo, O.; Sarkar, S. K.; Pejoux, C.; Ruhle, S.; Cahen, D.; Hodes, G. Chemical Bath Deposited CdS/CdSe-Sensitized Porous TiO_2 Solar Cells. *J. Photochem. Photobiol. A: Chem* **2006**, *181* (2−3), 306−313.

(8) Zhang, Q.; Guo, X.; Huang, X.; Huang, S.; Li, D.; Luo, Y.; Shen, Q.; Toyoda, T.; Meng, Q. Highly Efficient CdS/CdSe-Sensitized Solar Cells Controlled by the Structural Properties of Compact Porous TiO_2 Photoelectrodes. *Phys. Chem. Chem. Phys.* **2011**, *13* (10), 4659−4667.

(9) Braga, A.; Giménez, S.; Concina, I.; Vomiero, A.; Mora-Seró, I. Panchromatic Sensitized Solar Cells Based on Metal Sulfide Quantum Dots Grown Directly on Nanostructured TiO2 Electrodes. *J. Phys. Chem. Lett.* **2011**, *2* (5), 454−460.

(10) Santra, P. K.; Kamat, P. V. Tandem-Layered Quantum Dot Solar Cells: Tuning the Photovoltaic Response with Luminescent Ternary Cadmium Chalcogenides. *J. Am. Chem. Soc.* **2012**, *135* (2), 877−885.

(11) Santra, P. K.; Nair, P. V.; George Thomas, K.; Kamat, P. V. $CuInS_2$-Sensitized Quantum Dot Solar Cell. Electrophoretic Deposi-

tion, Excited-State Dynamics, and Photovoltaic Performance. *J. Phys. Chem. Lett.* **2013**, *4* (5), 722−729.
(12) Wang, G.; Wang, S.; Cui, Y.; Pan, D. A Novel and Versatile Strategy to Prepare Metal−Organic Molecular Precursor Solutions and Its Application in Cu(In,Ga)$(S,Se)_2$ Solar Cells. *Chem. Mater.* **2012**, *24* (20), 3993−3997.
(13) Kamat, P. V.; Tvrdy, K.; Baker, D. R.; Radich, J. G. Beyond Photovoltaics: Semiconductor Nanoarchitectures for Liquid-Junction Solar Cells. *Chem. Rev.* **2010**, *110* (11), 6664−6688.
(14) Pernik, D. R.; Tvrdy, K.; Radich, J. G.; Kamat, P. V. Tracking the Adsorption and Electron Injection Rates of CdSe Quantum Dots on TiO_2: Linked Versus Direct Attachment. *J. Phys. Chem. C* **2011**, *115* (27), 13511−13519.
(15) Hines, D. A.; Kamat, P. V. Quantum Dot Surface Chemistry: Ligand Effects and Electron Transfer Reactions. *J. Phys. Chem. C* **2013**, *117* (27), 14418−14426.
(16) Chakrapani, V.; Tvrdy, K.; Kamat, P. V. Modulation of Electron Injection in CdSe-TiO_2 System Through Medium Alkalinity. *J. Am. Chem. Soc.* **2010**, *132* (4), 1228−1229.
(17) Kongkanand, A.; Tvrdy, K.; Takechi, K.; Kuno, M. K.; Kamat, P. V. Quantum Dot Solar Cells. Tuning Photoresponse Through Size and Shape Control of CdSe-TiO_2 Architecture. *J. Am. Chem. Soc.* **2008**, *130* (12), 4007−4015.
(18) Christians, J. A.; Kamat, P. V. Trap and Transfer. Two-Step Hole Injection Across the Sb_2S_3/CuSCN Interface in Solid-State Solar Cells. *ACS Nano* **2013**, *7*, 7967−7974.
(19) Chakrapani, V.; Baker, D.; Kamat, P. V. Understanding the Role of the Sulfide Redox Couple in Quantum Dot-Sensitized Solar Cells. *J. Am. Chem. Soc.* **2011**, *133* (24), 9607−9615.
(20) Choi, H.; Kuno, M.; Hartland, G. V.; Kamat, P. V. CdSe Nanowire Solar Cells Using Carbazole as a Surface Modifier. *J. Mater. Chem. A* **2013**, *1* (18), 5487−5491.
(21) Maity, P.; Debnath, T.; Ghosh, H. N. Ultrafast Hole- and Electron-Transfer Dynamics in CdS−Dibromofluorescein (DBF) Supersensitized Quantum Dot Solar Cell Materials. *J. Phys. Chem. Lett.* **2013**, 4020−4025.
(22) Flaisher, H.; Tenne, R.; Hodes, G. Improved Performance of Cadmium Chalcogenide Photoelectrochemical Cells - Surface Modification Using Copper Sulfide. *J. Phys. D: Appl. Phys.* **1984**, *17* (6), 1055−1066.
(23) Hodes, G.; Manassen, J.; Cahen, D. Electrocatalytic Electrodes for the Polysulfide Redox System. *J. Electrochem. Soc.* **1980**, *127* (3), 544−549.
(24) Santra, P. K.; Kamat, P. V. Mn-Doped Quantum Dot Sensitized Solar Cells: A Strategy to Boost Efficiency Over 5%. *J. Am. Chem. Soc.* **2012**, *134* (5), 2508−2511.
(25) Luther, J. M.; Jain, P. K.; Ewers, T.; Alivisatos, A. P. Localized Surface Plasmon Resonances Arising from Free Carriers in Doped Quantum Dots. *Nature* **2011**, *10* (5), 361−366.
(26) Zaban, A.; Greenshtein, M.; Bisquert, J. Determination of the Electron Lifetime in Nanocrystalline Dye Solar Cells by Open-Circuit Voltage Decay Measurements. *ChemPhysChem* **2003**, *4* (8), 859−864.
(27) Wu, Y.; Wadia, C.; Ma, W.; Sadtler, B.; Alivisatos, A. P. Synthesis and Photovoltaic Application of Copper(I) Sulfide Nanocrystals. *Nano Lett.* **2008**, *8*, 2551−2555.
(28) Pileni, M. P. Reverse Micelles as Microreactors. *J. Phys. Chem.* **1993**, *97* (27), 6961−6973.
(29) Harris, C.; Kamat, P. V. Photocatalytic Events of CdSe Quantum Dots in Confined Media. Electrodic Behavior of Coupled Platinum Nanoparticles. *ACS Nano* **2010**, *4* (12), 7321−7330.
(30) Harris, C. T.; Kamat, P. V. Photocatalysis with CdSe Nanoparticles in Confined Media: Mapping Charge Transfer Events in the Subpicosecond to Second Timescales. *ACS Nano* **2009**, *3* (3), 682−690.
(31) Nave, S.; Paul, A.; Eastoe, J.; Pitt, A. R.; Heenan, R. K. What Is So Special about Aerosol-OT? Part IV. Phenyl-Tipped Surfactants†. *Langmuir* **2005**, *21* (22), 10021−10027.
(32) Baker, D. R.; Kamat, P. V. Tuning the Emission of CdSe Quantum Dots by Controlled Trap Enhancement. *Langmuir* **2010**, *26* (13), 11272−11276.
(33) Baral, S.; Fojtik, A.; Weller, H.; Henglein, A. Photochemistry and Radiation Chemistry of Colloidal Semiconductors. 12. Intermediates of the Oxidation of Extremely Small Particles of Cadmium Sulfide, Zinc Sulfide, and Tricadmium Diphosphide and Size Quantization Effects (a pulse radiolysis study). *J. Am. Chem. Soc.* **1986**, *108* (3), 375−378.
(34) Mishra, B.; Kumbhare, L. B.; Jain, V. K.; Priyadarsini, K. I. Pulse Radiolysis Studies on Reactions of Hydroxyl Radicals with Selenocystine Derivatives. *J. Phys. Chem. B* **2008**, *112* (14), 4441−4446.
(35) Kamat, P. V.; Dimitrijevic, N. M.; Fessenden, R. W. Photoelectrochemistry in Particulate Systems. 6. Electron-Transfer Reactions of Small CdS Colloids in Acetonitrile. *J. Phys. Chem.* **1987**, *91* (2), 396−401.
(36) Kamat, P. V.; Dimitrijevic, N. M.; Fessenden, R. W. Photoelectrochemistry in Particulate Systems. 7. Electron-Transfer Reactions of Indium Sulfide Semiconductor Colloids. *J. Phys. Chem.* **1988**, *92* (8), 2324−9.
(37) Dimitrijevic, N. M.; Kamat, P. V. Photoelectrochemistry in Particulate Systems. 8. Photochemistry of Colloidal Selenium. *Langmuir* **1988**, *4* (3), 782−4.
(38) Haase, M.; Weller, H.; Henglein, A. Photochemistry of Colloidal Semiconductors. 26. Photoelectron Emission from CdS Particles and Related Chemical Effects. *J. Phys. Chem.* **1988**, *92* (16), 4706−12.
(39) James, D. R.; Liu, Y.-S.; De Mayo, P.; Ware, W. R. Distributions of Fluorescence Lifetimes: Consequences for the Photophysics of Molecules Adsorbed on Surfaces. *Chem. Phys. Lett.* **1985**, *120* (4−5), 460−465.
(40) Choi, H.; Kamat, P. V. CdS Nanowire Solar Cells: Dual Role of Squaraine Dye as a Sensitizer and a Hole Transporter. *J. Phys. Chem. Lett.* **2013**, 3983−3991.